PERGAMON

Journal of Geodynamics 33 (2002) 353–376

JOURNAL OF GEODYNAMICS

www.elsevier.com/locate/jgeodyn

Progressive changes in strain patterns and fold styles in a deforming ductile orogenic wedge: an experimental study

Anupam Chattopadhyay[1]*, Nibir Mandal

Department of Geological Sciences, Jadavpur University, Calcutta 700 032, India

Received 8 November 2000; received in revised form 2 November 2001; accepted 4 December 2001

Abstract

Experiments with scaled, viscous pitch models demonstrate successive stages of growth (Stages I, II and III) of a ductile orogenic wedge with progressive deformation, which are kinematically as well as dynamically distinct from each other. In Stage I, vertical growth of the wedge is significant indicating dominant role of horizontal tectonic forces relative to the gravity forces. With progressive deformation, the wedge attains a stable height when Stage II begins. Migration of the wedge front in the transport direction maintaining constant height during Stage II implies a balance between gravity and horizontal contraction. In the last stage (Stage III), as the action of horizontal tectonic forces tend to weaken gradually, the wedge undergoes collapse under the influence of gravity. The three stages of wedge growth show characteristic strain distributions. In each stage, shape of the strain ellipses (indicator of finite strain at that stage) and their orientation (inclination of the ellipse major axes with respect to the direction of horizontal force) vary from hinterland toward foreland as well as from depth to shallower level. Strain ellipses at a given domain also exhibit changes in shape (aspect ratio) and orientation with advancing stages of deformation (Stages I to III). There is thus a spatial as well as temporal variation in strain observed in the deforming wedge. The experimental analysis is essentially two-dimensional as the flow of pitch in the third direction (parallel to the wedge front) is constrained. Experiments were also performed with layered, anisotropic viscous models to study the spatial and temporal variations of fold styles in a deforming wedge. In Stage I, shallow level folds are upright and symmetrical whereas those at depth are inclined to nearly recumbent and strongly asymmetrical, showing vergence toward foreland. The intermediate stage of wedge growth (Stage II) is characterised by development of 'back folds' and refolded folds, the development of which are consistent with the temporal variations of finite strain within a deforming wedge. New steeply inclined, foreland-vergent asymmetric folds develop in the extreme frontal part of the wedge during the gravity-induced collapse (Stage III).
© 2002 Elsevier Science Ltd. All rights reserved.

1. Introduction

Fold-and thrust belts (FTBs) are the zones of intense folding and thrusting that occur along the external margin of an orogenic belt. Complex interaction of folds and thrusts, fold interference at

* Corresponding author.
E-mail address: achattopadhyay@hotmail.com (A. Chattopadhyay).
[1] Present address: Geological Survey of India, Geochronology and Isotope Geology Division, 15 A&B, Kyd Street, Calcutta 700 016.

0264-3707/02/$ - see front matter © 2002 Elsevier Science Ltd. All rights reserved.
PII: S0264-3707(01)00079-5

different scales and spatial variation in fold styles are the characteristic structural features of these belts. Accretionary wedges formed at convergent plate margins are now considered as modern day analogues suitable for studying the evolution of ancient FTBs. Wedge tectonics generally involve deformation of sedimentary prisms resting on a rigid basement. In many orogenic belts, however, the base of deformation wedge lies at the mid-crustal level (Knott, 1994) and the basement is strongly deformed together with the cover rocks (Brown et al., 1986; Naha and Mohanty, 1988). In these types of thick-skinned tectonic settings, wedges probably evolve through deformation of a crustal section with detachment surfaces or distributed shear surfaces at depth.

Mechanics of accretionary wedges have been well studied and applied to the natural FTBs. Both analytical (Chapple, 1978; Stockmal, 1983; Willett, 1992) and experimental (Davies et al., 1983; Liu et al., 1992; Dixon and Liu, 1992) modelling have been carried out. Davies et al. (1983) and Dahlen (1984) investigated the mechanics of accretionary wedges by considering the deformation of brittle materials on a rigid substrate and the mode of internal deformation during formation of the wedge. Several workers have also modelled the development of tectonic wedges by deformation of ductile slabs resting on a rigid base. Cowan and Silling (1978) and Cloos (1982, 1984) have used viscous models to investigate material flow patterns within tectonic wedges whereas Stockmal (1983) and Willett (1992) have assumed rigid-plastic rheology of the wedge material for their theoretical models and showed the positions of high strain within a deforming wedge. Analytical and experimental models have also shown that several physical factors: e.g. basal friction, initial surface slope, basal slope etc. play important roles in the development of tectonic wedges (Mulugeta, 1988; Liu et al., 1992; Koyi, 1995; Mandal et al., 1997).

From different FTBs, there are recorded observations that fold styles show a systematic spatial variation (Fyson, 1971). Folds in high grade gneisses (deeper level rocks) are dominantly recumbent whilst inclined to upright folds are observed in shallow level rocks such as phyllites and slates. Asymmetric, inclined folds generally verge toward foreland. However, hinterland-vergent folds ('back-folds') have been reported (Brown et al., 1986; Macaya et al., 1991). Systematic temporal variations in fold styles have also been observed e.g. superposition of later upright folds on earlier recumbent folds (Fyson, 1971). These spatial and temporal variations in fold styles can be explained by considering the progressive changes in strain patterns in a growing orogenic wedge.

This paper presents an experimental study on progressive development of a ductile orogenic wedge. The study indicates three stages of wedge growth that are characterised by distinctly different internal strain distributions in two dimensions. A series of experiments was conducted to study the spatial and temporal variations of fold style within a growing wedge. The experiments indicate that in viscous models the fold styles are consistent with strain distributions in different stages of wedge growth.

2. Kinematics of a ductile wedge

2.1. Experimental method

Experiments were conducted with homogeneous pitch models. Pitch (road tar) is a viscous material and at room temperature ($\sim$30 °C), its viscosity is in the range of 10^5 Pas (Jaeger, 1969).

Detailed rheological data on pitch are, however, not available. In spite of this limitation, pitch was used as model material because of its flowage under gravity.

A mass of pitch was kept inside a glass-walled long rectangular box for about 30 min, so that pitch could flow to take the shape of the container, with a dimension of 40 × 12 × 4 cm. This pitch block was then placed on a wooden platform with a thin (~ 2 mm thick) layer of soft painter's putty separating the pitch from the wooden base. This low-strength putty layer acted essentially as a surface of detachment during deformation of the model. In a separate series of experiments, the pitch block was directly placed on the wooden plate. In this case pitch stuck to the base very firmly, leading to a condition of total coherence or 'welding' at the base of the block. Deformation of these models, as discussed later, showed geologically unrealistic wedge geometry. For studying progressive stages of wedge development, the upper edge of the pitch block was, in some cases, marked with a horizontal marker line (Fig. 1). In different experiments, marker points, circular marks and square grids were painted on the vertical longitudinal face of the pitch block to study the internal flow patterns and strain distribution in the deformation wedge.

Models were deformed in a pure shear box by moving a screw-driven plate form one side at a rate of 0.01 cm/s. At this speed the wedge formed in front of the moving plate had a stable average surface slope of 10–12°, which is geologically realistic (Chapple, 1978; Mitra and Sussman, 1997) (see 'Discussion' for details).

2.2. Stages of wedge development

Based on the nature of wedge growth, the entire course of development of a wedge is divided into three stages (Fig. 2). These stages also have characteristic strain distribution as discussed later. In the following discussion, 'rear' means the model edge in contact with the pushing wall ('hinterland' of the FTBs) while 'front' means the undeformed part on the opposite side of the model ('foreland' of FTBs).

Stage I: with the shortening of the model from one side, a wedge formed in front of the moving plate reflecting a strong horizontal stress gradient. The wedge grew in height and the surface slope of the model (initially horizontal), increased rapidly (Figs. 2 and 3b). Distinguishing feature of Stage I is that vertical growth of the wedge was important and horizontal forces were dominant relative to gravity forces.

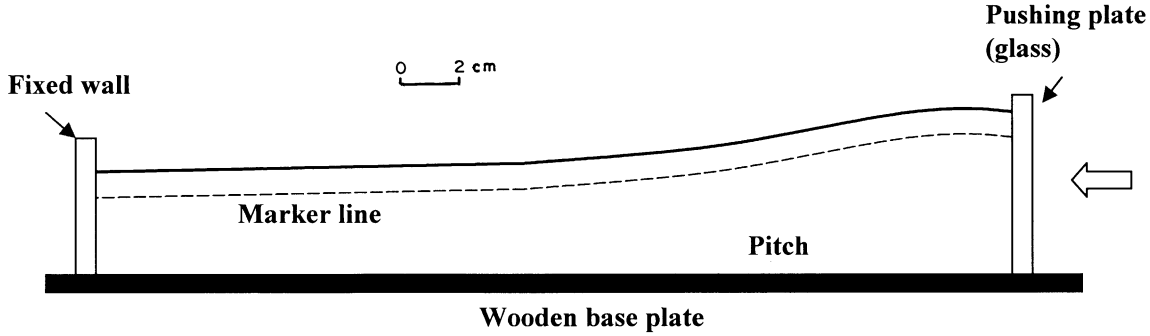

Fig. 1. Schematic sketch of experimental set-up for deformation of pitch models.

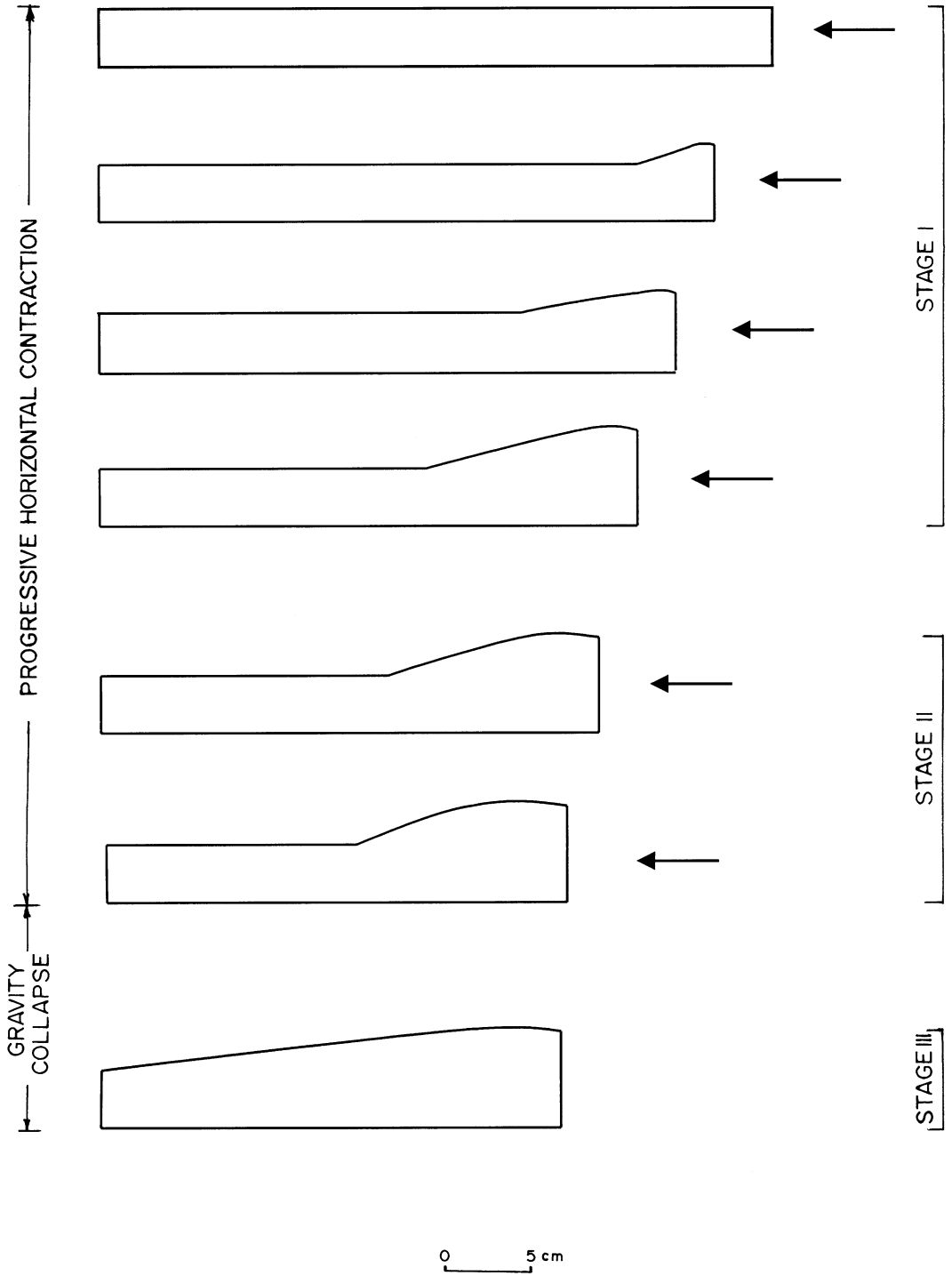

Fig. 2. Successive stages of wedge growth in initially rectangular pitch models, resting on a horizontal base (see text for details of the stages).

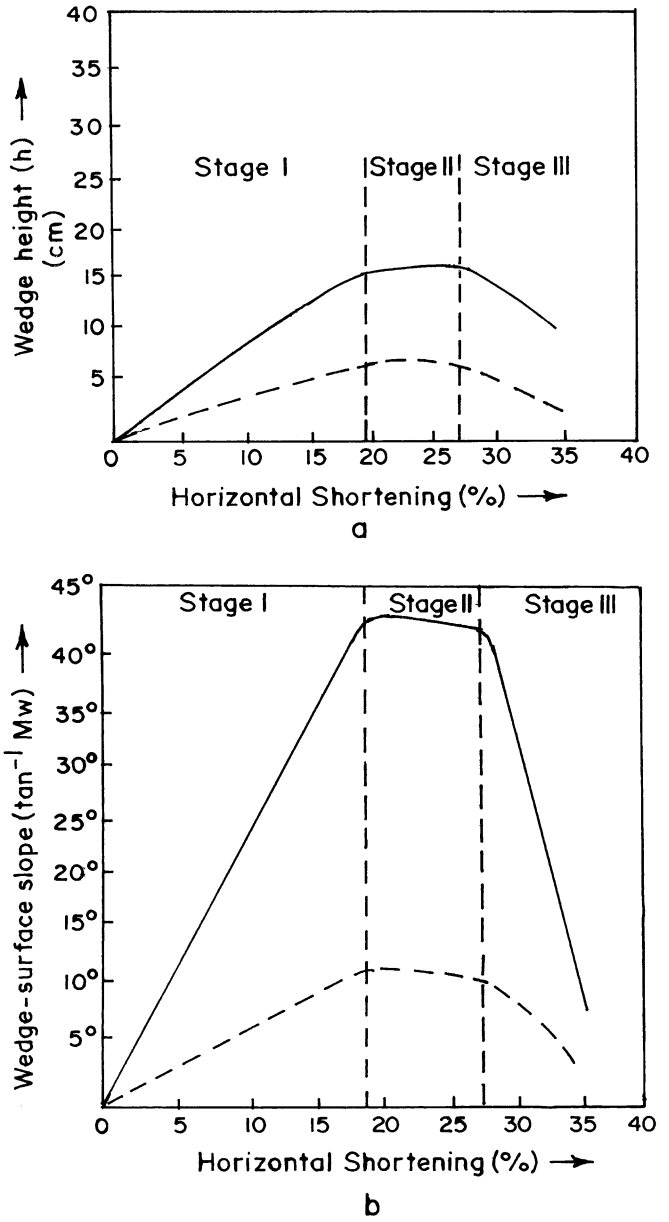

Fig. 3. Change in (a) wedge height and (b) wedge surface slope with bulk shortening. Dashed lines represent wedge with a ductile detachment (putty layer) at base and solid lines represent wedge 'welded' with base (no detachment).

Stage II: as the wedge grew in height, gravity forces became progressively more important and finally, stopped the upward viscous flow of pitch. Consequently, vertical growth of the wedge ceased and the wedge attained a stable height (Figs. 2 and 3a). With further shortening, the wedge advanced toward foreland, maintaining a stable surface slope and maximum height (Fig. 3). It is to be noted that for a constant rate of shortening, models with 'coherent' or 'welded' base showed

much higher surface slope than those with low-strength detachment surface at base. It thus appears that a basal detachment, either in the form of low angle sole thrust (in brittle wedges) or as a decollement surface (in ductile wedges), is essentially present in a geologically realistic deformation wedge.

Stage III: the experimental run was terminated by gradually decreasing the rate of shortening, to simulate the waning phase of an orogenic cycle. During this period, gravity force dominated over horizontal 'push' and the wedge started to collapse under gravity (Fig. 2). The wedge slope and height steadily decreased (Fig. 3) by gravity-induced internal flow of material from hinterland to foreland. This changing flow pattern considerably modified the strain distribution within the wedge. This is demonstrated by the changes in aspect ratio of the strain ellipses (indicating changes in finite strain, assuming plane strain condition) and inclination of their major axes (representing projection of XY plane of the finite strain ellipse on the XZ plane) with progressive deformation, in a given domain within the wedge. Details of the changes will be discussed in a later section.

2.3. Material flow patterns in the wedge

Particle paths were traced out from the displacements of a number of marker points on the vertical faces of the model. The displacements were measured with respect to a reference frame set at the stationary wall in front of the model. The displacement trajectories (particle paths), in general, had gentle inclination toward hinterland (Fig. 4a). During the transition between Stage I and Stage II, points at the intermediate depth level moved faster than those lying above.

During gravity-induced collapse (Stage III), particles in the elevated rear part of the wedge moved downward with significant vertical displacement components. At depth, the particle paths had a more pronounced horizontal displacement component (Fig. 4b). There was a general concave upward form of particle paths in the frontal part of the wedge, similar to that described by Ramberg (1991, Fig. 10). These particle path analyses were essentially two-dimensional and do not reveal movement of more internal particles.

2.4. Strain distribution within the wedge

To observe the possible variation in the finite strain in different parts of the deforming wedge, circular marks were painted on the lateral face of the homogeneous pitch block, with the help of a marker stamp and white plastic paint. With progressive deformation of the wedge, the circles were deformed to ellipses of variable shape (aspect ratio) and orientation (inclination of the major axes). The finite strain at any stage of deformation is obtained from the aspect ratio of the strain ellipses and the orientation of the XY plane of finite strain is indicated by the inclination of their major axes, if a plane strain condition is assumed. Following is a brief description of the spatial variation in strain pattern within the deforming wedge and the temporal changes in finite strain with progressive deformation (Stages I to III).

Stage I: finite strain in the wedge varied with depth. The XY planes of finite strain were nearly vertical at shallow levels and became more and more inclined at depth (Fig. 5a), with a prominent forelandward vergence. The zone of internal deformation in the wedge described a tapered profile—vertically wider at the rear and narrower towards front. The girdle of maximum finite strain (calculated from aspect ratio of ellipses) was located at the core of the wedge (Fig. 6).

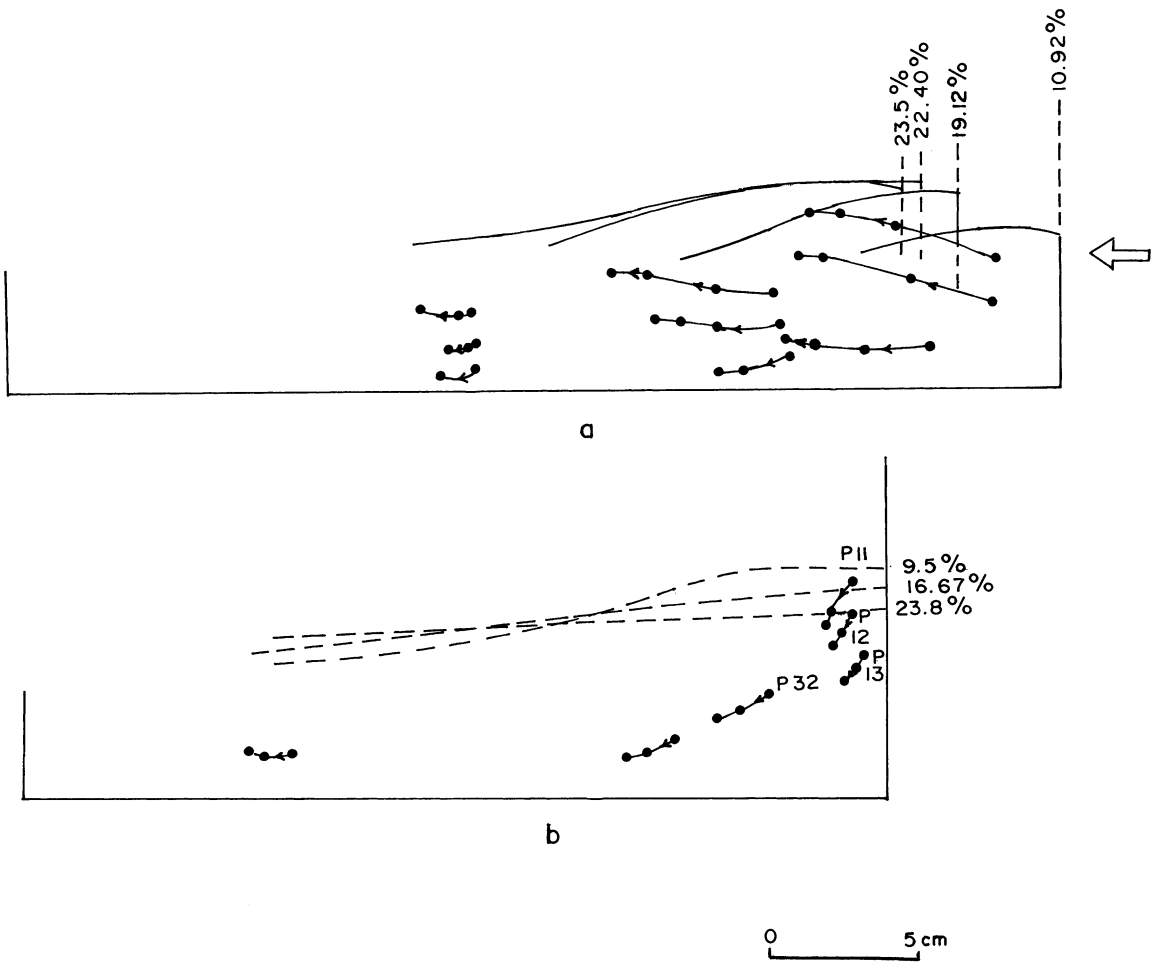

Fig. 4. Particle paths in course of wedge development during horizontal shortening. (a) Stages I and II (active shortening); (b) Stage III (gravity-induced collapse). Shortening from the right.

Stage II: at Stage II, the XY planes of finite strain at the shallower levels rotated to verge backward (toward hinterland) and the strain distribution became strongly heterogeneous (Fig. 5b). This back rotation of strain ellipses might be a result of an instantaneous back-shear (top towards hinterland) component, created by faster rate of flow of material at intermediate depth in the rear part of the wedge, as observed from particle paths (cf. Fig. 4a).

Fig. 7 shows how finite strain changed at different points within the wedge (marked a, b,. . .e) in Stage II during progressive deformation. At points a and b, the axes of the strain ellipse rotated backward. At the same time, finite strain first decreased and then increased (indicated by the changing shape of the ellipse) with progressive shortening. This rear central part of the wedge thus acts as a domain of pulsating strain. In contrast, at depth (points d,e) finite strain continuously increased and strain ellipses continuously rotated toward foreland during progressive deformation (Figs. 5b and 7).

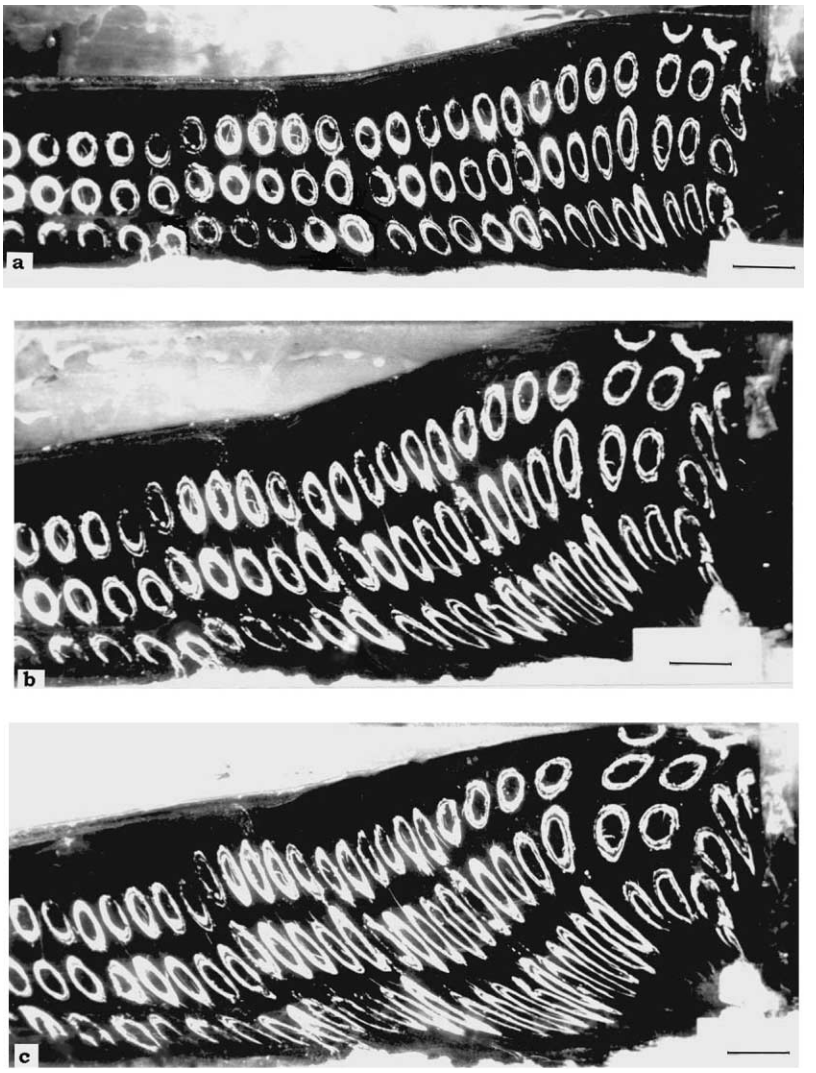

Fig. 5. Strain patterns in successive stages of wedge development in homogeneous pitch model. (a) Stage I, (b) Stage II and (c) Stage III. Shortening from the right. Scale bar = 1 cm.

Stage III: due to gravity-induced collapse of the wedge, the existing strain pattern was strongly modified by internal flow of material in Stage III. The back-vergent ellipses were strongly flattened and further rotated toward hinterland (Fig. 5c). Local finite strain below this domain decreased down to almost zero whereas ellipses at further depth and also in the frontal part of the wedge continued to flatten during Stage III. Fig. 8 schematically shows the changes in shape and orientation of finite strain ellipses in different domain of the wedge during gravity collapse. At point a, the back-vergent ellipses (produced in Stage II) were further flattened and back-rotated. At point b, on the other hand, the vertical sagging effected in decreasing the aspect ratio of the strain ellipse, indicating a decrease in finite strain (Figs. 6 and 8). This is the only domain where a pulsating type of deformation took place with progressive shortening of the wedge. Compression

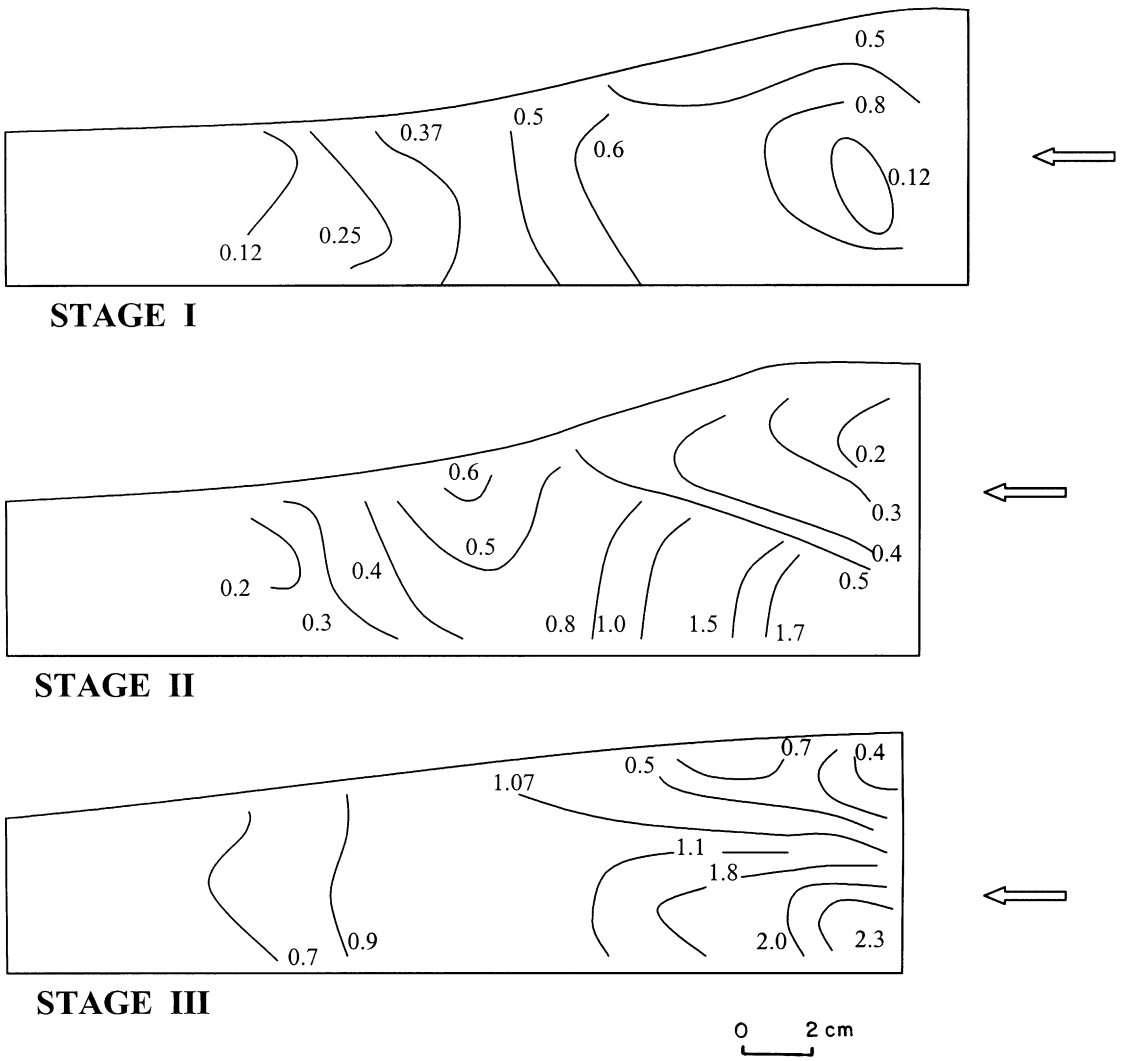

Fig. 6. Finite strain map of different stages of wedge growth calculated from experiments. Shortening from the right.

parallel to the XY plane of ellipses at this position signified this as a possible domain of coaxial refolding, as will be discussed later. In the rear, deeper part of the wedge (point c), finite strain increased continuously and XY planes continued to rotate forelandward. In the frontal part (points d and e), the finite strain increased with increased vergence of XY planes towards foreland. It is interesting to see that in the deeper frontal part of the wedge (point d), finite strain was negligible during Stage II. Internal flow of material towards foreland (cf. Fig. 4b) in Stage III imparted a significant amount of strain in this domain even when there was no active horizontal 'push'.

A separate set of experiments was carried out with square marker grids painted of the vertical side face of the wedge, just before the onset of Stage III. Square grid was used to delineate the

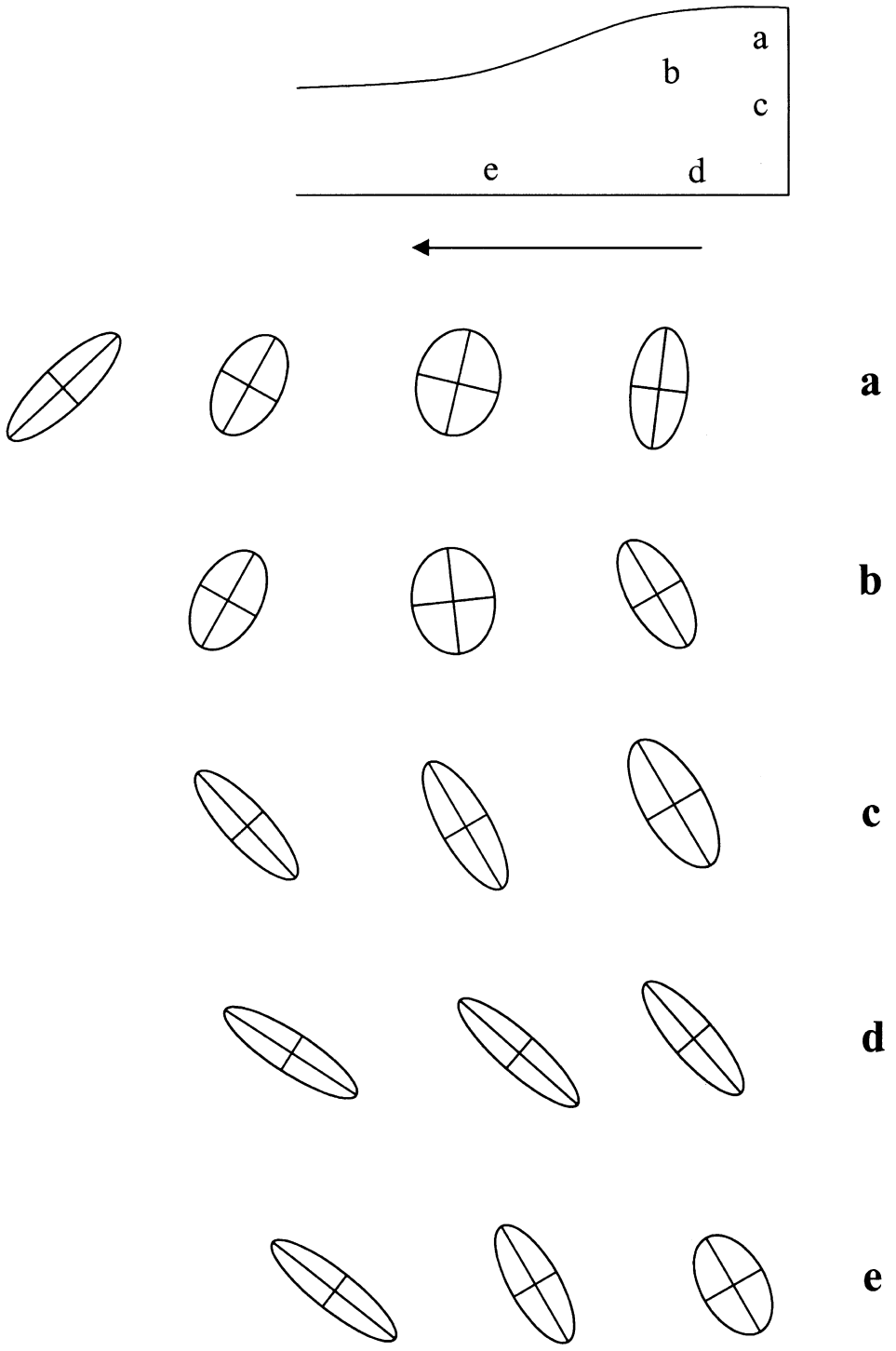

Fig. 7. Temporal variation of finite strain at different points (a,b,c..) in the wedge from Stage I to Stage II. Note the changing nature of both the aspect ratio and the orientation of strain ellipses. Schematic diagram, not to scale.

heterogeneity of deformation in vertical and horizontal directions, in different domains at Stage III. Gravity collapse of the wedge during Stage III showed the following features (Fig. 9).

1. A strong back-shear developed at the rear upper part of the wedge.
2. Pure shear-type horizontal extension at the core of the wedge.

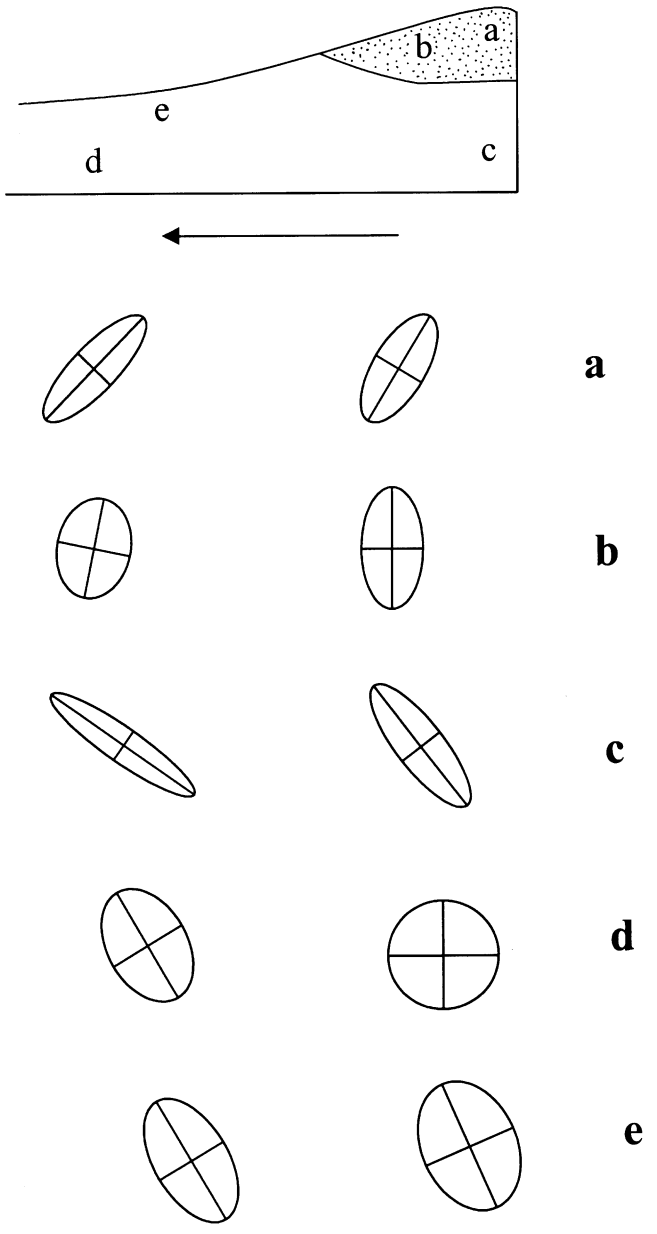

Fig. 8. Temporal variation of finite strain from Stage II to Stage III. The dotted area represents domain of decreasing finite strain during Stage III. Schematic diagram, not to scale.

3. Strong horizontal shortening and vertical extension in the frontal part of the wedge, possibly due to flowage of material form hinterland to foreland due to internal gravity-induced adjustments.

3. Fold styles in a deforming wedge

The experiments with homogeneous pitch models described in the previous section revealed the progressive changes of the strain pattern within a ductilely deforming orogenic wedge. However, direct observation of these progressive changes of strain in the field would be rather uncommon. On the other hand, spatial and temporal variations in the shape and orientation of folds in an orogenic belt are commonly observed. The changes in shape and orientation of the strain ellipses

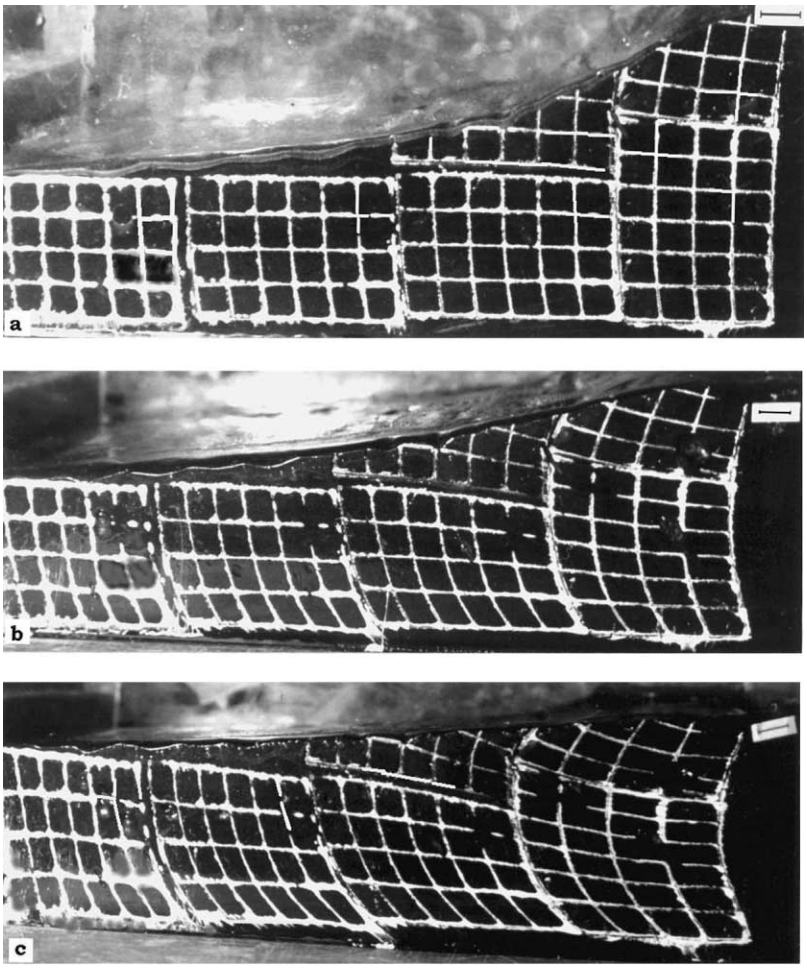

Fig. 9. Distortion of square grid marks during gravity-induced collapse of the wedge (Stage III). Grids were marked on the wedge face after Stage II. Wedge surface slope was slightly enhanced to enhance the effect of gravity-induced sagging of the wedge. Shortening from right. Scale bar = 1 cm.

in different domains of a deforming wedge have a direct bearing on the changing geometry of folds in those domains. A series of experiments were therefore carried out with layered anisotropic models under boundary conditions similar to those during the earlier experiments, to see the possible correlation of the variation in fold style with the changing pattern of strain.

3.1. Experimental method

Layered, heterogeneous anisotropic models made of plasticine, painter's putty and pitch were used to simulate varying patterns of folding within a ductilely deforming wedge. Standard commercial brand of plasticine (modelling plasticlay) was used to simulate competent layers. The rheological parameters and exact composition of this plasticine are uncertain, but its non-Newtonian viscous property was confirmed from the stress vs strain rate curve of plasticine blocks subjected to uniaxial compression test. For simulating incompetent matrix, a soft painter's putty, prepared by mixing talcum powder and wheel bearing grease in 1:1 volume ratio, was used. The putty was weakly viscous (viscosity possibly in the range of 10^3–10^4 Pa s), but its flowage property was not very strong so as to account for the influence of gravity-induced flow on the fold structures. The plasticine-putty models were initially rectangular in cross-section with length, width and thickness (height) of 35–40, 12–14 cm and 6–8 cm, respectively. Models were of two types: (1) thin single layers embedded within putty at different depth levels, to avoid contact strain between the layers (Fig. 10a) and (2) closely spaced plasticine multilayer with lubricated layer- interfaces, embedded entirely within the incompetent material (Fig. 10b). To account for the effect of gravity forces on the evolving fold patterns, we carried out a separate set of experiments with a special type of composite model. A narrow slab of widely spaced single-layered plasticine-putty model was embedded within a rectangular block of pitch so that it was partially enclosed by pitch (Fig. 10c). During deformation, the strong gravity-induced flow of pitch (especially in Stages II and III) significantly modified the shape and orientation of the evolving fold structures. This gave us a qualitative idea of the possible influence of gravity forces on the fold styles in a deforming wedge.

Models were deformed in a pure shear box with a screw-driven piston form one side. Rate of horizontal shortening was approximately 0.01 cm/s. Succesive stages of fold development and wedge growth was photographed through the transparent glass walls. After final deformation, the model was longitudinally cut with the help of a fine steel wire and internal structures were revealed.

3.2. Fold development in the deforming wedge

3.2.1. Folding in Stage I

Spatial variation in fold style during Stage I of wedge development is shown in a synoptic diagram (Fig. 11), combining results of different experiments. In the frontal part, gentle, symmetric folds occurred at shallow level and were underlain by undeformed layers. Foreland-vergent, strongly asymmetric folds localised in the zone between intensely deformed hinterland and weakly deformed foreland. This zone was followed towards hinterland, by a zone of symmetric inclined folds. Apart from this lateral variation, there was a systematic variation of fold styles with depth. From the photograph (Fig. 13a) it is evident that in general, shallow level folds were

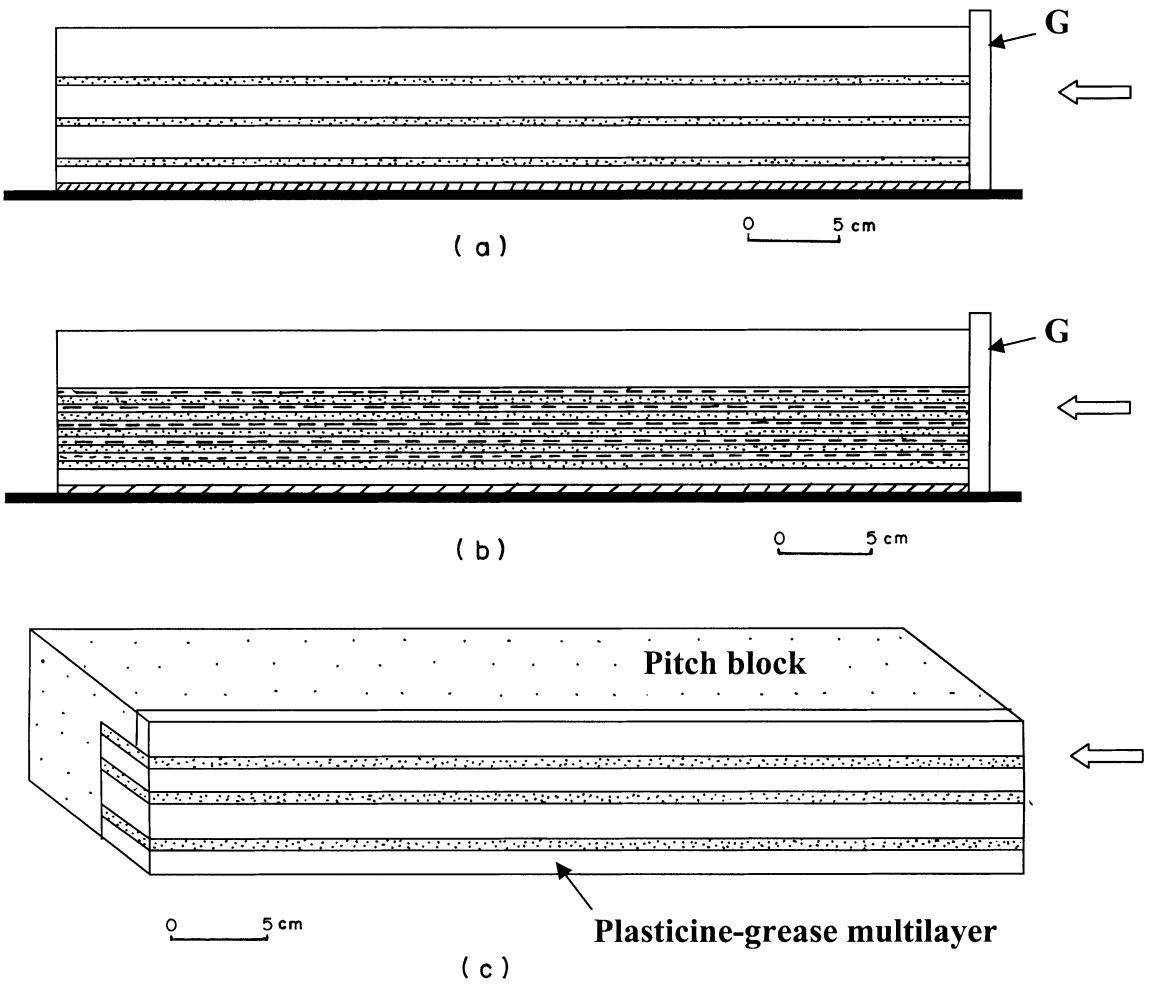

Fig. 10. Types of layered models to simulate the folds. (a) Model with widely spaced plasticine layers in putty; (b) closely spaced plasticine multilayer embedded in putty; (c) composite model of plasticine, putty, pitch. Dense stipple: stiff plasticine, light stipple: pitch, blank space: grease, dash: softer plasticine, G: pushing plate.

symmetric and upright. At intermediate depth, folds were symmetric to asymmetric with steeply hinterland-dipping axial planes whereas folds at greater depth were always strongly asymmetric with a prominent foreland-vergence. This type of spatial variation in fold styles has been reported in geological literature (Fyson, 1971; Sanderson, 1979).

It is to be noted that the axial planes of folds in different domains of the wedge in Stage I (Fig. 13a) are generally parallel to the XY planes of the strain ellipses in the corresponding positions in a Stage I ductile pitch wedge (cf. Fig. 5a). During the run of the experiments, it was observed that folds developed at depth in the rear part of the wedge were initially symmetric. Axial planes of these folds rotated towards foreland similar to the rotation of the XY plane of strain ellipses in that domain, due to strong shear component near the base. As a result, folds became strongly asymmetric and foreland-vergent. On the other hand, at shallower level, the

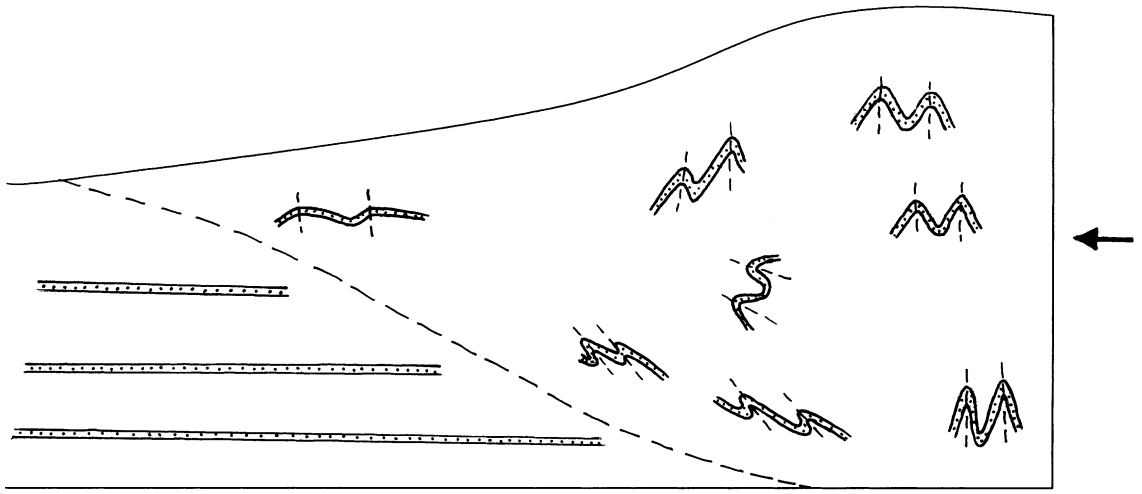

Fig. 11. A synoptic diagram of fold styles in Stage I. Sketch from parts of Fig. 13 (not to scale).

shear drag was absent. Therefore shallow level folds formed and remained as symmetric, upright to inclined folds.

3.2.2. Folding in Stage II

Folds formed in different parts of the wedge in Stage I, were greatly modified during Stage II, due to superposition of later folds on earlier (Stage I) folds, body rotation of some earlier folds etc., just as the strain ellipses of Stage I were modified in Stage II (cf. Figs. 5a and 6). Some new folds also developed during Stage II. Pre-eminent among them were back-vergent asymmetric folds (axial planes dipping toward foreland) at shallow depth (Fig. 13c). This type of 'back-folds' has been reported by Macaya et al. (1991). Rotation of the XY planes of the finite strain ellipse in this domain during Stage II (Fig. 5b) can explain the development of these folds. During growth of the ductile wedge in Stage II, the upward viscous flow of model material is counterbalanced by the gravity-induced flow at depth—creating a temporary stability in the height and surface slope of the wedge. To maintain plane strain condition, material at intermediate depth flows towards foreland at a faster rate than that at shallower level at the later part of Stage II. This produces an effective reverse shear drag at the shallower level in the rear part of the wedge and rotates the XY planes of strain ellipses towards hinterland. Also, incremental strain ellipses in this domain, during Stage II, must be back-vergent. Axial planes of the evolving folds thus become hinterland-vergent and give rise to asymmetric 'back folds'.

Fold interference in the form of coaxial refolding of earlier axial planes (Type III interference of Ramsay and Huber, 1987) or as superposition of new folds on the limbs of early (Stage I) folds were a characteristic feature of Stage II. Fold interference occurred in response to the temporal variation in local strain pattern with change in wedge geometry. Interfering folds showed a systematic variation of orientation of axial planes in the wedge (Fig. 12). In the hinterland part, at an intermediate depth level, interfering folds had horizontal to subhorizontal axial planes and they were superposed on the limbs of early (Stage I) upright to steeply inclined symmetric folds (location **1** in Fig. 13b; second white layer from top). This shows how coaxial refolding of an

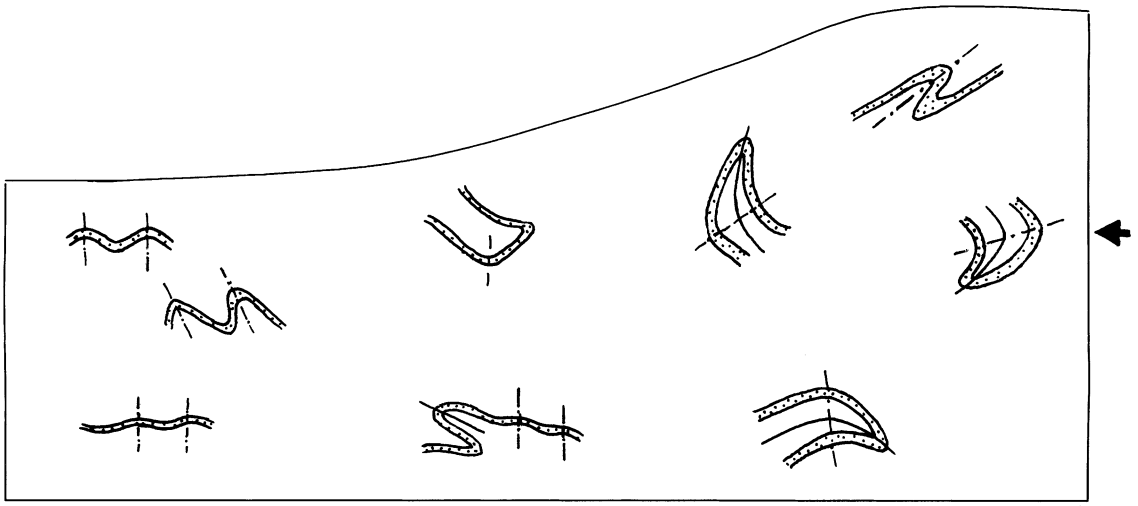

Fig. 12. Spatial variation of the geometry of interfering folds in Stages II and III. Solid lines show the axial planes of early (Stage I) folds and dashed lines represent the axial planes of later (superposed) folds. Shortening from right. Synoptic sketch, not to scale.

early fold can take place in some domains during same ongoing deformation. It should be noted that in this domain the shape of the strain ellipses changed during Stage II (cf. Fig. 5a and b). Thus the rear central part of a ductile wedge can be a domain of pulsating deformation. On the other hand, at depth, later upright folds were superposed on the gently dipping limb of an inclined to recumbent fold (location **2** in Fig. 13b). In the frontal part, Stage II folds are mostly upright. Fig. 12 shows a synoptic diagram combining all varieties of fold interference in different domains of a wedge during Stage II. All the types did not necessarily develop in any single experiment.

3.2.3. Folding in Stage III

It has already been mentioned that the strain pattern of Stage I and Stage II was greatly modified during Stage III due to dominant vertical sagging at the rear part of the wedge and forelandward flow of materials at depth, under the influence of gravitational forces. From Fig. 9 it is evident that there was an increment of horizontal shortening in the foreland part of the wedge during Stage III, even when there was no 'active' push from hinterland. In layered anisotropic models (composite plasticine-putty-pitch models in this case), this resulted in the development of weak, symmetric, upright folds in the far frontal part (Fig. 14a; location **1**). Fig. 14b and c shows the modification of fold patterns due to gravity-collapse in Stage III. Fig. 14b is a section of the composite layers outside the pitch block, less affected by the gravity-induced flow of pitch and represents the fold pattern upto Stage II. Fig. 14c, on the other hand, is a deeper section encased within the pitch block and it shows the possible modification of Stage II folds by gravity-induced flow. Due to significant gravity-induced vertical sagging in the rear and central part of the wedge, steep limbs of asymmetric Stage II folds are superposed by smaller recumbent Stage III folds (location **1**, Fig. 14c). Inclined symmetric folds developed in Stage II at intermediate depth, were tightened (Fig. 14c, location **2**) during Stage III.

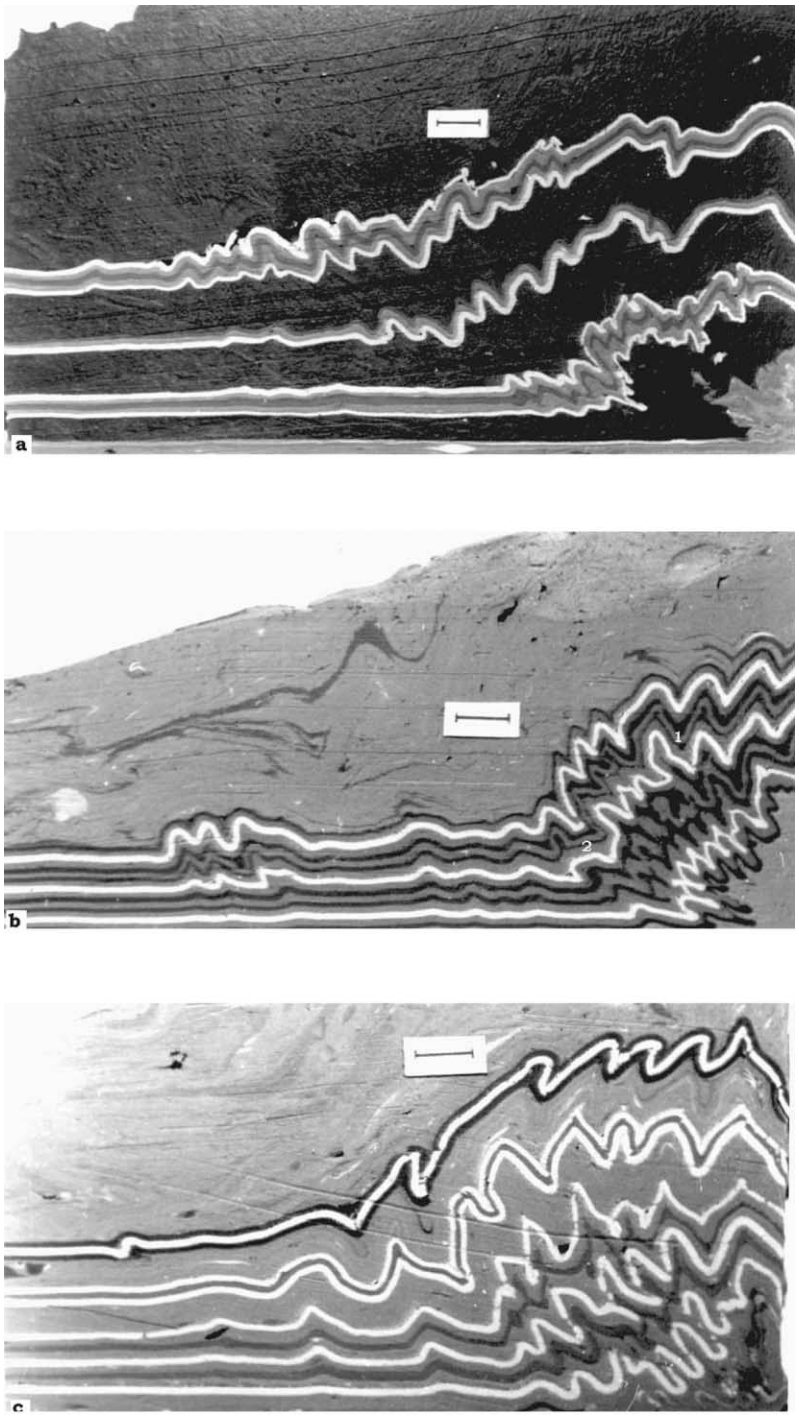

Fig. 13. (a) Fold styles in the wedge in Stage I; (b) superposition of newer folds on earlier (Stage- I) folds in Stage II; (c) development of 'back fold' in Stage II (topmost layer in the rear part of the wedge). Shortening from right in all cases. Scale bar = 1 cm.

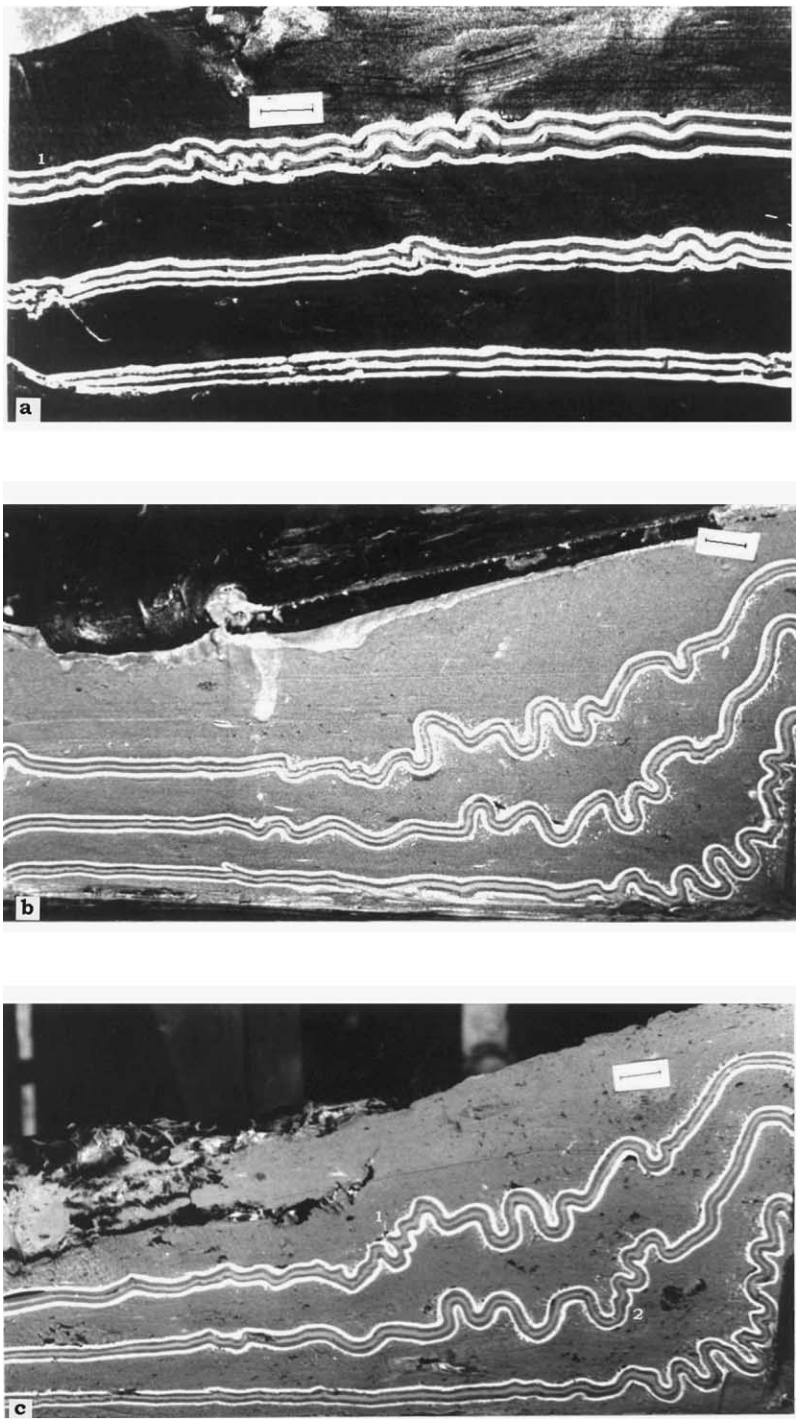

Fig. 14. (a) Development of weak symmetric folds in the shallow level layers (loc.1) in Stage III; (b) and (c) superposition of later recumbent folds on the steep limbs of earlier folds (loc.1) and tightening of symmetric folds at depth (loc. 2). Scale bar = 1 cm.

4. Discussion

Experiments with homogeneous pitch block were generally scaled to nature. To verify this, we have calculated the different model ratios (after Hubbert, 1937), as listed in Table 1. The rheological data were obtained either by direct measurement in the laboratory, or from published literature.

From the tabulated data we obtained the three fundamental model ratios, considered most important for scaling, as under:

(i) model ratio of length (λ) = 4.0×10^{-6}
(ii) model ratio of time (τ) = 1.3×10^{-11}
(iii) model ratio of mass (μ) = $\delta\lambda^3 = 2.0 \times 10^{-17}$.

The model ratios given above clearly indicate that pitch models used in the present experiments were generally scaled to nature, within some degree of approximation. Geometric similarity was achieved by the model length ratio ($\lambda = 4.0 \times 10^{-6}$). Kinematic similarity was achieved by the model ratio of time ($\tau = 1.3 \times 10^{-11}$) and by ensuring that the sequence of development of structures with progressive shortening is similar to that in natural FTBs. For achieving dynamic similarity, Hubbert (1937) argued that: (1) the model should have a mass distribution similar to that of the original (natural) one, defined by the model ratio of mass (μ) and (2) different forces (e.g. gravity, inertia, viscous resistance, stress etc.) acting on the model and the corresponding forces operating in its natural counterpart should be proportional, the constant of proportionality being the model ratio of force (ϕ). Hubbert also showed that this very definition of dynamic similarity creates an insurmountable problem to experimental modelling. If two body forces viz. gravity and inertia coexist in the model, as they generally do, and both have to satisfy

Table 1
Model dimensions and scaling ratios

Quantities	Model (pitch)	Nature	Model ratio
1. Acceleration due to gravity	$g_m = 9.81$ m/s^2	$g_n = 9.81$ m/s^2	$g_m/g_n = 1$
2. Length (parallel to the direction of shortening)	$l_m = 40$ cm	$l_n = 100$ km	$\lambda = l_m/l_n = 4.0 \times 10^{-6}$
3. Rate of shortening	$t_m = 0.01$ cm/s	$t_n = 1$ cm/year (after Cotton and Koyi, 2000)	$\tau = 1.3 \times 10^{-11}$ (model ratio of time)
4. Average density of material	$d_m = 1.15$ gm/cc	$d_n = 2.6$ gm/cc[a]	$\delta = d_m/d_n = 0.45$
5. Average viscosity	$\xi_m = 1.5 \times 10^5$ Pa s (after Jaeger, 1969)	$\xi_n \approx 2.9 \times 10^{21}$ Pa.s[b]	$\xi = 5.1 \times 10^{-17}$

[a] Average density of the upper crustal material is approximated as the average of the density of granite (2.7 gm/cc, after Hubbert, 1937) and that of supracrustal sedimentary rocks (2.5 gm/cc, after Cotton and Koyi, 2000).

[b] Roughly estimated viscosity data as indicated by Haskel and by Gutenberg (both cited in Hubbert, 1937). Similar data has been used by Shaw (1969). CGS units have been converted to SI units for viscosity.

the condition of dynamic similarity, then we come across a situation where $\tau = \lambda^{1/2}$. Thus the two fundamental model ratios - the model ratio of length and of time—cannot be chosen independently (Hubbert, 1937, p. 1473). To overcome this problem, Hubbert suggested that in case of very slowly moving viscous or plastic models, the forces due to inertia can be neglected without causing significant error. Consequently, dynamic similarity can be achieved if model ratios of length (λ), mass (μ) and time (τ) are chosen arbitrarily and forces viz. stress, pressure, shear strength, viscosity etc. are made to conform to the ratio $\phi = \mu. = \delta\lambda^3$ (Hubbert, 1937, p. 1489). In the present case, we have used viscous models under very slow rate of shortening. Therefore we assumed negligible inertial forces following Hubbert's argument. The condition of dynamic similarity was achieved, in our experiments, by the model ratio of mass ($\mu = 2.0 \times 10^{-17}$). Due to lack of detailed rheological data of pitch as well as that of crustal material, many of the force ratios could not be calculated in the present case. However, we attempted to calculate viscosity ratio. Using the approximate viscosity data of earth by Haskel, by Gutenberg (both cited in Hubbert, 1937) and by Shaw (1969, Fig. 11) and of pitch (model) by Jaeger (1969), we found the approximate ratio of viscosity to be in the range of 10^{-17} (Table 1). On the other hand, ratio of viscosity (ξ), calculated from the fundamental ratios (after Hubbert, 1937) is:

$$\xi = \mu\lambda^{-2}\tau = \delta\lambda\tau = 2.3 \times 10^{-17},$$

which is of the same order of magnitude as the actual ratio (Table 1). The conditions of dynamic similarity was therefore generally satisfied in our experiments, although the lack of well constrained viscosity data of crustal material leaves a degree of approximation in the scaling calculations.

Hubbert (1937) suggested that a material suitable for simulating a mountain belt, should be weak enough, so that a small cube ($\sim$3 cm side) of the material collapses or flows under its own weight. Pitch is a viscous material, which flows under its own weight very readily and hence fulfils the strength criteria suggested by Hubbert, at least qualitatively. This shows that the pitch models approximately satisfied the dynamic similarity criteria. Results of these experiments can thus be applied to the natural thick-skinned fold belts.

The layered plasticine-putty models were not appropriately scaled as plasticine was probably too hard to deform under the slow and weak viscous drag of putty, even under significant gravitational forces. Again, model ratios could not be calculated as neither the rheological parameters nor the exact composition of plasticine was known. However, experiments with composite models of plasticine-putty and pitch could qualitatively show the influence of gravity on the evolving fold structures, especially in the last stage, when gravity forces played dominant role. The changing fold patterns in all these experiments match very well with the changing patterns of strain found in scaled experiments. Thus the results are scientifically predictable and can be qualitatively applied to natural fold-thrust belts.

The experimental results provoked some ideas on the spatial and temporal variations of fold geometry in an orogenic belt. Fyson's (1971) observation that shallower level folds should be upright and deeper level folds should be recumbent, seems to be generally valid. This type of spatial variation is quite consistent with the strain distribution and fold pattern in Stage I (Figs. 5a and 13a). However, the present experiments indicate that the fold styles may be more complex in

the advanced stages of deformation, due to temporal variation in fold style. In Stage II, hinterland-vergent, inclined folds form at a shallower level, consistent with the orientation of XY-planes of finite strain ellipses in this domain. This type of "back folds" has been described earlier from many orogenic provinces (Macaya et al., 1991). The present experiments show that these folds can develop in some domains during the same orogenic movement that generates foreland-vergent folds elsewhere in the orogenic belt. In natural conditions, the XY plane of finite strain may be defined by a cleavage/metamorphic fabric axial planar to the folds. Rotation of these material planes (cleavage/schistosity) may not necessarily track the rotation of geometric XY planes leading to the folding of schistosity etc. during progressive deformation which is commonly observed in natural FTBs.

Coaxial refolding of early folds is very common in almost all the orogenic belts. But a question always remains whether they develop in a single progressive deformation or in successive discrete deformations. In the latter case, it is difficult to explain how compression takes place parallel to the axial plane of a fold in the same deformation. Assumption that the later fold is a shear fold (Ramsay, 1967) may not always hold good. This problem can be tackled to a certain extent by considering the temporal changes in strain distribution within a deforming wedge. As discussed earlier, a large domain occurs in the rear central part of the wedge, where the finite strain decreases from Stage I to Stage II while it increases everywhere else in the wedge. This happens because due to the increased effect of gravity-induced sagging, the XY planes of incremental strain in this domain make a high angle with the XY planes of finite strain, in Stage II. This generates compression parallel to the XY plane of finite strain in this domain (Fig. 5b). As folds in Stage I form with axial planes parallel to the XY plane of finite strain, they suffer compression parallel to the axial planes in Stage II, leading to co-axial refolding (Fig. 13b). A good match between the strain pattern and the superposed structures observed in the experiments indicates that coaxial refolding can be produced during progressive deformation, in certain domains.

The last phase of deformation in many orogenic belts forms weak kink-folds with sub-horizontal axial planes (Naha and Halyburton, 1974). These structures can be explained by strong gravity-induced sagging in rear part of the orogenic wedge in Stage III, which may lead to kinking/folding of steeply dipping (or sub-vertical) structural planes (e.g. schistosity) in this fashion. The superposition of small recumbent folds on the steeper limb of Stage II inclined fold in our experiments (Fig. 14b and c) illustrates this process. Again, Ramberg's (1991) analysis and the present experiments show that due to gravity-induced adjustments in the late phase, material in the deeper part of the deforming wedge flows toward foreland in an upward concave path. This causes strain and folding in the yet undeformed layers in the foreland. In our experiments, forelandward flow of pitch was restricted by the frontal buttress plate, causing a pure-shear type situation that produced symmetric upright folds in the foreland. In natural situations, however, the flow would be free toward foreland and significant non-coaxial deformation will occur, resulting in the development of asymmetric, foreland-vergent folds even after the orogenic 'push' is over.

The present experimental analysis was essentially two-dimensional, the third side (perpendicular to the transport direction) being buttressed by glass walls. The lateral flow of material in this direction could change the strain pattern to some extent. However, we have assumed that in natural situation, the deforming wedge would be self-similar across the width of the orogenic belt, for all practical purposes.

Our models were deformed by moving a rigid planar plate from rear and the boundary velocity was kept constant with depth. However, in natural situations the boundary velocity of tectonic regimes may be more complex and may vary with depth. We conducted a few experiments with curved rigid walls. Except for the folds in the near vicinity of the wall, fold style in general was not much different than that in the present experiments.

In our experiments, vertical flow of pitch was uniform along the width (perpendicular to shortening direction) of the model and created cylindrical wedge front. The wedge collapsed in Stage III with major flow perpendicular to the overall wedge trend. But orogenic wedges may not be laterally uniform and gravity-induced flow during post-orogenic phase may be much more complex. Therefore, later folds may not be strictly coaxial with the earlier folds during structural superposition.

Rate of shortening (0.01 cm/s) in our experiments was the lowest rate that we could achieve with the apparatus used. The shape of the pitch wedge produced at this rate of shortening was, however, geologically realistic. Chapple (1978) calculated the surface slope (α) and the basal slope (θ_0) in the deforming wedge of Valley and Ridge Province to be 8.26° and 3°, respectively, indicating a wedge taper of 11.26°. Mitra and Sussman (1997) presented retrodeformable sections of Sevier fold-and-thrust belt which indicate a wedge taper of at least 12–15° at an advanced stage of deformation (Fig. 2, Mitra and Sussman, 1997). In the present series of experiments, we have kept the base of the deforming wedge horizontal, due to experimental constraints. Therefore, in our experiments, the total wedge taper is equal to the surface slope of the wedge, produced by deformation. Thus, a stable average slope of around 12° of the wedge surface, is geologically well approximated. Similar approximation i.e. the wedge taper being defined by the surface slope only, has been used by other workers (Davies et al., 1983, Liu et al., 1992) in experiments with non-cohesive Coulomb wedge. However, presence of a significant basal slope may influence, to some extent, the geometry of the folds in the deforming ductile wedge. Several authors (Chapple, 1978; Boyer, 1995; Mitra, 1997) have shown that basal slope is an important factor to the development of FTBs. Similar influence of basal slope on the architecture of thrusts in brittle wedges has been observed earlier by us (Mandal et al., 1997). Had there been a significant basal slope in our models, there could be a quantitative change in the stable height of the wedge and orientation of folds. Spatial variation in fold style with respect to the inclined base, however, would be broadly similar.

It has already been mentioned that a deformation wedge can be modelled with either brittle, non-cohesive Coulomb material or with materials of viscous/plastic rheology. Deformation of a brittle, non-cohesive wedge is accommodated by thrusting. The architecture of thrusts within such wedges has already been investigated by us using dry, non-cohesive sand (Mandal et al., 1997). Therefore, to investigate fold styles and strain distribution, we have chosen viscous model materials (pitch, plasticine, putty etc.) to simulate a ductilely deforming wedge. In natural condition, the crustal material probably behaves in a more complex manner, resulting in near-simultaneous development of folds and thrusts.

5. Conclusions

Structural evolution of a ductilely deforming orogenic wedge consists of three kinematically as well as dynamically distinct stages with characteristic strain patterns. In the earliest stage, horizontal

tectonic forces play a dominant role resulting in the development of the wedge form. In the intermediate stage, horizontal 'push' and gravity induced vertical sagging play equally significant roles while at the last stage, when horizontal 'push' slackens, the wedge deforms mainly under the influence of gravity. During the interaction of gravity and horizontal tectonic forces, the wedge maintains its shape by complex internal flow of material toward foreland. This induces significant changes in the strain pattern within the wedge from one stage to another. Finite strain generally increases with progressive deformation but in some locales, it first increases and then decreases resulting in pulsating strain domains. In conformity with these spatial and temporal variations of strain, styles of folding in different domains in the wedge also show systematic spatial and temporal variations. In general, shallow level folds are symmetric, upright folds while strongly asymmetric, foreland-vergent, gently inclined folds form at depth. Asymmetric, upright to symmetric, inclined folds concentrate at intermediate depth. At a later stage of deformation, due to interaction of gravity and horizontal tectonic forces, more complex structures viz. back folds, coaxial refolding of earlier folds etc. develop at different depths. In the last stage, when the wedge collapses under the influence of gravity, symmetric, upright to asymmetric, foreland-vergent folds develop in the yet undeformed foreland part, due to strong forelandward flow of material in the deeper part of the wedge even as there is no active orogenic push.

Acknowledgements

We express our sincere thanks to Professor S.K. Ghosh, who introduced us to experimental structural geology and helped us with numerous technical advises during the work. Thanks are due to T. Dutta for drafting the figures. The University Grants Commission, Government of India provided financial support in the form of research fellowship to A.C. The Jadavpur University, Calcutta, India provided the infrastructural facilities for the research.

References

Boyer, S.E., 1995. Sedimentary basin taper as a factor controlling the geometry and advance of thrust belts. Am. J. Sci. 295, 1220–1254.

Brown, R.L., Jouneay, J.M., Larry, S.L., Murphy, D.C., Ree, C.J., 1986. Obduction, backfolding and piggyback thrusting in the metamorphic hinterland of the southeastern Canadian Cordillera. J. Struct. Geol. 8, 255–268.

Chapple, W.M., 1978. Mechanics of thin-skinned fold-and-thrust belts. Bull. Geol. Soc. Am 89, 1189–1198.

Cloos, M., 1982. Flow melanges: numerical modelling and geologic constraints on their origin in the Fransiscan subduction complex, California. Bull. Geol. Soc. Am 93, 330–345.

Cloos, M., 1984. Flow melanges and the structural evolution of accretionary wedges. Geol. Soc. Am. Spcl. Pap 198, 71–79.

Cotton, J.T., Koyi, H.A., 2000. Modelling of thrust fronts above ductile and frictional detachments: application to the structures in the Salt Range and Potwar Plateau. Pakistan. Bull. Geol. Soc. Am. 112, 351–363.

Cowan, D.S., Silling, R.M., 1978. A dynamic, scaled model of accretion at trenches and its application for the tectonic evolution of subduction complexes. J. Geophys. Res. 83, 5389–5396.

Dahlen, F.A., 1984. Non-cohesive critical coulomb wedges: an exact solution. J. Geophys. Res. 89, 10125–10133.

Davies, D.M., Suppe, J., Dahlen, F.A., 1983. Mechanics of fold-and-thrust belts and accretionary wedges. J. Geophys. Res. 88, 1153–1172.

Dixon, J.M., Liu, S., 1992. Centrifuge modelling of the propagation of thrust belts. In: McClay, K.R. (Ed.), Thrust Tectonics. Chapman & Hall, London, pp. 53–69.

Fyson, W.K., 1971. Fold attitudes in metamorphic rocks. Am. J. Sci. 270, 373–382.
Hubbert, M.K., 1937. Theory of scale models as applied to the study of geologic structures. Bull. Geol. Soc. Am. 48, 1459–1520.
Jaeger, J.C., 1969. Elasticity, Fracture and Flow. 3rd Edition. Methuen, London.
Knott, S.D., 1994. Structures, kinematics and metamorphism in the Linguside complex, southern Apenines. Italy. J. Struct. Geol 16, 1107–1120.
Koyi, H., 1995. Mode of internal deformation in sand wedges. J. Struct. Geol. 17, 293–300.
Liu, H., McClay, K.R., Powell, D., 1992. Physical models of thrust wedges. In: McClay, K.R. (Ed.), Thrust Tectonics. Chapman & Hall, London, pp. 71–81.
Macaya, J., Gonzalez-Lodeiro, F., Martinez-Catalan, J.R., Alvarez, F., 1991. Continuous deformation, ductile thrusting and backfolding of cover and basement in the Sierra de Guadarrama, Hercynian Orogen of central Spain. Tectonophys. 191, 309–921.
Mandal, N., Chattopadhyay, A., Bose, S., 1997. Imbricate thrust spacing: experimental and theoretical analyses. In: Sengupta, S. (Ed.), Evolution of Geological Structures in Micro- to Macro- Scales. Chapman & Hall, London, pp. 143–165.
Mitra, G., 1997. Evolution of salients in a fold-and-thrust belt: the effects of sedimentary basin geometry, strain distribution, and critical taper. In: Sengupta, S. (Ed.), Evolution of Geological Structures in Micro- to Macro- Scales. Chapman & Hall, London, pp. 59–90.
Mitra, G., Sussman, A.J., 1997. Structural evolution of connecting splay duplexes and their implications for critical taper: an example based on geometry and kinematics of the Canyon Range culmination, Sevier Belt, central Utah. J. Struct. Geol 19, 503–521.
Mulugeta, G., 1988. Modelling the geometry of coulomb thrust wedges. J. Struct. Geol. 10, 847–859.
Naha, K., Halyburton, R.V., 1974. Late strain systems deduced from conjugate folds and kink bands in the 'Main Railo Syncline', Udaipur district, Rajasthan, India. Bull. Geol. Soc. Am. 85, 251–256.
Naha, K., Mohanty, S., 1988. Response of basement and cover rocks to multiple deformation: a study from the Precambrians of Rajasthan, western India. PreCamb. Res. 42, 77–96.
Ramberg, H., 1991. Numerical simulation of spreading nappes, sliding against basal friction. Tectonophys. 188, 159–186.
Ramsay, J.G., 1967. Folding and Fracturing of Rocks. McGraw-Hill, NY.
Ramsay, J.G., Huber, M.I., 1993. Techniques of Modern Structural Geology. vol. 2: Folds and Fractures. Academic Press, NY.
Sanderson, D.J., 1979. The transition from upright to recumbent folding in the Variscan fold belts of southwest England: a model based on the kinematics of simple shear. J. Struct. Geol. 1, 171–180.
Shaw, H.R., 1969. Rheology of basalt in the melting range. J. Petrol. 10, 510–535.
Stockmal, G.S., 1983. Modelling of large-scale accretionary wedge deformation. J. Geophys. Res. 88, 8271–8287.
Willett, S.D., 1992. Dynamic and kinematic growth and change of a coulomb wedge. In: McClay, K.R. (Ed.), Thrust Tectonics. Chapman & Hall, London, pp. 19–31.